Separation and Purification Technology 306 (2023) 122678

Contents lists available at ScienceDirect

Separation and Purification Technology

journal homepage: www.elsevier.com/locate/seppur

A novel C_2H_2-selective microporous Cd-MOF for C_2H_2/C_2H_4 and C_2H_2/CO_2 separation

Yong-Zhi Li [a], Rajamani Krishna [c], Fan Xu [a], Wan-Fang Zhang [b], Yanwei Sui [a], Lei Hou [b,*], Yao-Yu Wang [b], Zhonghua Zhu [d]

[a] School of Materials and Physics, China University of Mining and Technology, Xuzhou 221116, PR China
[b] Key Laboratory of Synthetic and Natural Functional Molecule of the Ministry of Education, Shaanxi Key Laboratory of Physico-Inorganic Chemistry, College of Chemistry & Materials Science, Northwest University, Xi'an 710069, PR China
[c] Van 't Hoff Institute for Molecular Sciences, University of Amsterdam, 1098 XH Amsterdam, the Netherlands
[d] School of Chemical Engineering, The University of Queensland, Brisbane 4072, Australia

ARTICLE INFO

Keywords:
Metal-organic framework
Gas adsorption
Adsorption selectivity
Breakthrough experiment

ABSTRACT

Separation of acetylene (C_2H_2) from ethylene (C_2H_4) or carbon dioxide (CO_2) is a vital and difficult task in petrochemical industry. Owing to the similar physical properties, it is very challenging to synthesize target porous materials with standout separation performance. Herein, we report the utilization of an isophthalic acid linker substituted with pyridine groups to construct a novel microporous Cd-MOF $[Cd_2(dpip)_2(DMF)(H_2O)]\cdot DMF\cdot H_2O$ (**1**). The Cd-MOF features suitable pore surfaces modified by carboxyl oxygen atoms to contact closely with C_2H_2 molecules, which leads to considerable C_2H_2 adsorption ability of 124.4 $cm^3\ g^{-1}$ at 100 kPa and 298 K, significantly higher than C_2H_4 and CO_2. Experimental breakthroughs indicate the Cd-MOF can efficiently separate C_2H_2 from C_2H_2/CO_2, C_2H_2/CH_4, and C_2H_2/C_2H_4 mixtures. The productivities of $\geq$ 99.996% C_2H_4 purity calculated on the basis of simulated transient breakthroughs for 1/99 C_2H_2/C_2H_4 were determined to be 27.72 and 60.77 L kg^{-1} at 298 and 273 K, respectively. Molecular simulation demonstrates the pivotal role of the multiple interactions in the framework for C_2H_2.

1. Introduction

The separation and purification of light hydrocarbons is a crucial process for the production of clean energy and high-purity chemicals, but it is also an expensive and energy-intensive technology [1–3]. Among them, acetylene (C_2H_2) is used as important fuel gas in welding/cutting, and is also the basic feedstock to produce several commodity chemicals [4–6]. C_2H_2 mainly originates from the partial combustion of methane (CH_4) or hydrocarbon cracking process, and faces the problem presenting with by-products including carbon dioxide (CO_2) and CH_4 [7–9]. Therefore, separating C_2H_2 from CH_4 or CO_2 mixtures is of industrial importance for obtaining high purity C_2H_2 for the manufacture of value-added products. In another aspect, ethylene (C_2H_4), as the largest feedstock in petrochemical industry, inevitably contains some impurities such as C_2H_2. Trace C_2H_2 would poison the catalyst in the polymerization process of C_2H_4, which needs to be removed to an acceptable level of below about 40 ppm of C_2H_2 [10–12]. Hence, it is needed to purify C_2H_4 from C_2H_2/C_2H_4 mixtures. However, due to similar physicochemical properties and molecular dimensions [13], the solvent extraction or cryogenic distillation techniques commonly used in industry for C_2H_2/CO_2 and C_2H_2/C_2H_4 separations are energy-intensive processes and also cause severe environmental problems. In contrast, porous material-based physical adsorption separation method provides alternatives with a low-energy and simultaneously achieves a green environmental effect [14–16]. The development of new kinds of porous media is highly desirable to target excellent performance of gas separation.

Metal-organic frameworks (MOFs), self-assembled by organic connectors with metal clusters/ions, are the state-of-the-art porous solid materials because of their powerful predictability as well as tunability on pore size/shape [17–20]. In the past two decades, MOFs have aroused widespread attention in catalysis [21], magnetism [22], drug delivery [23], conductivity [24], and gas separation [25]. Especially for gas separation, MOFs exhibit advantages in accurately controlling the pore size and pore chemical environment through reticular chemistry and crystal engineering strategies [26–30]. Targeted design and synthesis of

* Corresponding author.
E-mail address: lhou2009@nwu.edu.cn (L. Hou).

https://doi.org/10.1016/j.seppur.2022.122678
Received 29 September 2022; Received in revised form 10 November 2022; Accepted 13 November 2022
Available online 17 November 2022

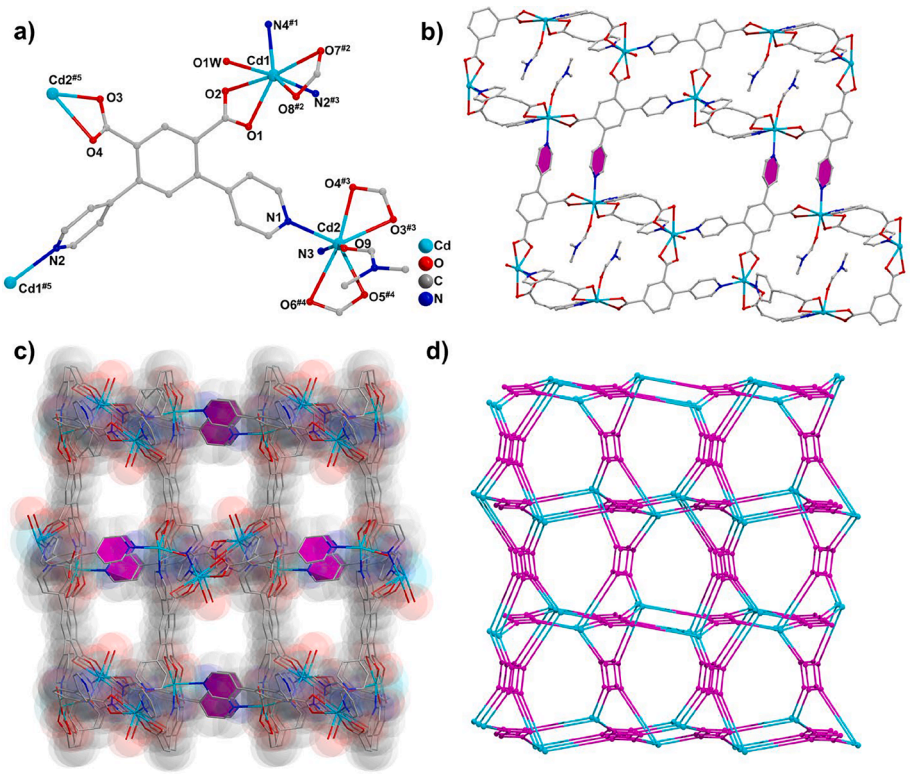

Fig. 1. a) Coordination environment of Cd^{2+} ions; b) 2D corrugated layers on the *ac* plane; c) 3D porous framework; d) topological net. (For interpretation of the references to colour in this figure legend, the reader is referred to the web version of this article.)

MOF materials according to the differences in molecular size and polarity of the components to be separated is of paramount importance to achieve high gas separation efficiency [31–32]. For example, for gas mixtures with different molecular sizes, the size-exclusion strategy is effective [33,34]. However, for C_2H_2 and CO_2 with similar molecular sizes, additional functional sites (such as Lewis N sites and open metal sites) need to be introduced to enhance the interactions between the framework and one of the gases to achieve separation [35–37]. It is worth noting that the adsorption intensity of active sites should be moderate, and strong strength will result in higher desorption energy, increasing energy consumption in regeneration [38–39]. Therefore, accessible suitable binding sites combing suitable pore sizes in MOFs could significantly enhance the adsorption and separation ability toward C_2H_2.

It is known that pyridylcarboxylate ligands usually form structurally diverse MOFs, where the carboxylic acid groups have multiple coordination modes, while pyridine group can form stable coordination bonds with M(II) transition metal ions. In this work, we employ a pyridinecarboxylic ligand, 4,6-di(pyridin-4-yl) isophthalic (H_2dpip), for MOF construction. The ligand is that the 4- and 6- positions of the benzene ring in isophthalic acid are replaced by pyridine groups, which can coordinate with the metal ions in four directions that tend to afford open frameworks, which is conducive to the transfer of adsorbates in the process of adsorption and separation. Herein, we developed a novel Cd-MOF, $[Cd_2(dpip)_2(DMF)(H_2O)]\cdot DMF\cdot H_2O$ (**1**) via reacting H_2dpip and Cd^{2+} ions under solvothermal conditions. The Cd-MOF has channels modified by carboxyl oxygen atoms, which not only shows higher adsorption capacity for C_2H_2 compared to CO_2, C_2H_4, and CH_4, but also displays dynamic separation for C_2H_2/CO_2, C_2H_2/C_2H_4, and C_2H_2/CH_4 mixtures.

2. Experimental

2.1. Materials and methods

The details of this section were presented in Supporting Information.

2.2. Synthesis of $[Cd_2(dpip)_2(DMF)(H_2O)]\cdot DMF\cdot H_2O$ (1)

The mixture of $Cd(NO_3)_2\cdot 4H_2O$ (0.0308 g, 0.10 mmol) and H_2dpip (0.0154 g, 0.05 mmol) in DMF (4 mL), ethanol (1 mL), and trifluoroacetic acid (0.05 mL) was capped in a 25 mL vessel and heated at 115 °C for 72 h. After cooling to room temperature, colourless block crystals were obtained (yield: 53%, based on H_2dpip). Anal. Calcd for $C_{42}H_{38}Cd_2N_6O_{12}$: C, 48.34; H, 3.67; N, 8.05%. Found: C, 48.15; H, 3.98; N, 8.01%.

3. Results and discussion

3.1. Structural analysis

The Cd-MOF **1** crystallizes in the monoclinic $P2_1/n$ space group, and includes two Cd(II) ions, two deprotonated dpip ligands, one coordinated water molecule, and one coordinated DMF molecule in the asymmetric unit. The Cd^{2+} center is seven-coordinated in a pentagonal bipyramid geometry formed by four O atoms from two carboxylate linkers (Cd-O = 2.270–2.603 Å), two pyridyl N atoms (Cd-N = 2.277–2.378 Å), and one O atom of coordinated solvent molecule (Fig. 1a). Four Cd(II) ions are connected by dpip ligands to form ring-like SBUs, and which are connected by pyridyl rings in ligands to form a two-dimensional (2D) waved layer parallel to the *ac* plane (Fig. 1b). The adjacent layers are further cross-linked by dpip ligands with Cd(II) ions, forming a porous 3D framework (Fig. 1c). The pore size distribution is estimated to be about 15.1–16.5 Å according to the PoreBlazer 4.0 (Figure S1) [40]. The void of framework calculated using a probe of 1.2

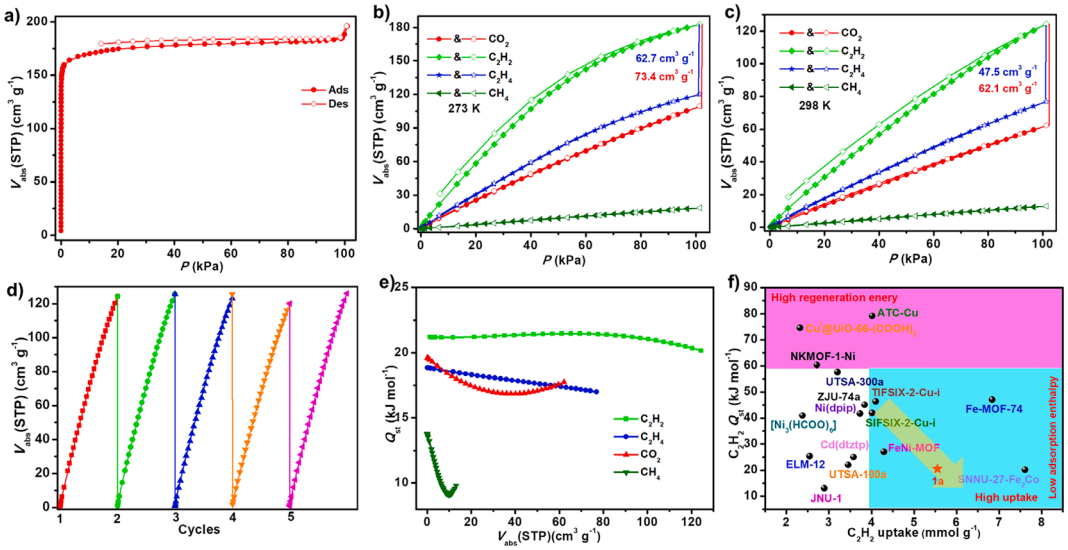

Fig. 2. a) Adsorption isotherm of N_2 at 77 K; b) and c) adsorption isotherms of CO_2, C_2H_2, C_2H_4, and CH_4 for **1a** at 273 and 298 K; d) cycled C_2H_2 adsorption of **1a** at 298 K; e) adsorption heats of **1a**; f) comparison of C_2H_2 uptakes and adsorption heats between **1a** and other MOFs at 298 K.

Å by PLATON program is 55.6% (including coordinated solvent molecules), showing high porosity. The framework possesses a (4,4)-connected ($4^2{\cdot}8^4$)-*pts* topology, while both Cd(II) ions and ligands are regarded as 4-connection nodes (Fig. 1d).

3.2. PXRD and TGA

The sample purity was verified by the consistency of PXRD between the measured and simulated (Figure S2). TGA shows an 8.8% weight reduction before 120 °C, resulting from the decrease of free water and DMF molecules (calcd. 8.7%) [41,42]. Next, the weight loss of 8.3% from 120 to 250 °C corresponds to the loss of coordinated water and DMF molecules (calcd. 8.7%) (Figure S3). PXRD of **1** shows the thermal stable temperature at about 300 °C as well as the good stability in common organic solvents (acetone, toluene, methanol, acetonitrile, DMF, DMSO), water and different aqueous solutions with pH = 3–10 for 1 day (Figure S4). The desolvated sample **1a** was gained by soaking **1** in CH_2Cl_2 for 48 h, and then heating at 150 °C for 4 h under vacuum, as characterized by the PXRD and TGA analyses.

3.3. Gas adsorption

The permanent porosity of **1a** was investigated by nitrogen (N_2) adsorption experiment at 77 K. As illustrated in Fig. 2a, it exhibits a fully reversible typical type-I adsorption behavior, with the maximum uptake of 195.9 $cm^3\ g^{-1}$ at 100 kPa. The fitted Brunauer-Emmett-Teller and Langmuir surface areas are 698 and 800 $m^2\ g^{-1}$ (Figure S5). Moreover, the distribution of pore size localizes in the range of 9–12 Å based on the Horvath-Kawazoe model (Figure S6), matching well with the calculated pore dimensions derived from crystal structure.

The high porosity and bare carboxyl O atoms in the pores of **1a** prompted us to explore C_2H_2 storage and separation behaviors. Single-component equilibrium adsorption isotherms of C_2H_2, C_2H_4, CO_2, and CH_4 on **1a** were recorded at 273, 298 and 313 K (Fig. 2b, 2c, S7 and Table S3), which show a higher uptake for C_2H_2 than other gases. The single-component isotherms revealed that **1a** adsorbs 124.4/182.8 $cm^3\ g^{-1}$ of C_2H_2, 76.8/120.0 $cm^3\ g^{-1}$ of C_2H_4, 62.2/109.4 $cm^3\ g^{-1}$ of CO_2, and 13.1/18.7 $cm^3\ g^{-1}$ of CH_4, and the uptake ratio of C_2H_2/CO_2, C_2H_2/C_2H_4, and C_2H_2/CH_4 reached 2/1.67, 1.62/1.52, and 9.5/9.8 at 298 and 273 K under 100 kPa, respectively. Although the C_2H_2 uptake value of **1a** at 298 K is under than some benchmark MOFs like MIL-160 (191 $cm^3\ g^{-1}$) [43], MOF-505(148 $cm^3\ g^{-1}$) [44], and SNNU-27-Fe (182 $cm^3\ g^{-1}$) [16], but is superior or comparable with many famous MOFs, such as JNU-2 (103 $cm^3\ g^{-1}$) [8], NUM-9 (103 $cm^3\ g^{-1}$) [45], UTSA-100a (95 $cm^3\ g^{-1}$)[46], NPU-1(114 $cm^3\ g^{-1}$)[47], and UPC-60-Cl (100 $cm^3\ g^{-1}$) [48], suggesting promising candidate for C_2H_2 storage. Remarkably, the uptake ratio of C_2H_2/CO_2 at 298 K is superior to some reported MOFs, such as UTSA-74a (1.52 at 298 K) [49], FJU-6-TATB (1.89 at 296 K) [50], [Ni(tzba)$_{0.5}$(F)(bpy)] (1.45 at 298 K) [51], and FJI-H8-Et (1.75 at 298 K) [35], indicating great separation potential application to address this challenging gas mixtures. Five adsorption–desorption cycle experiments for C_2H_2 reflect great repeatability and regeneration performance

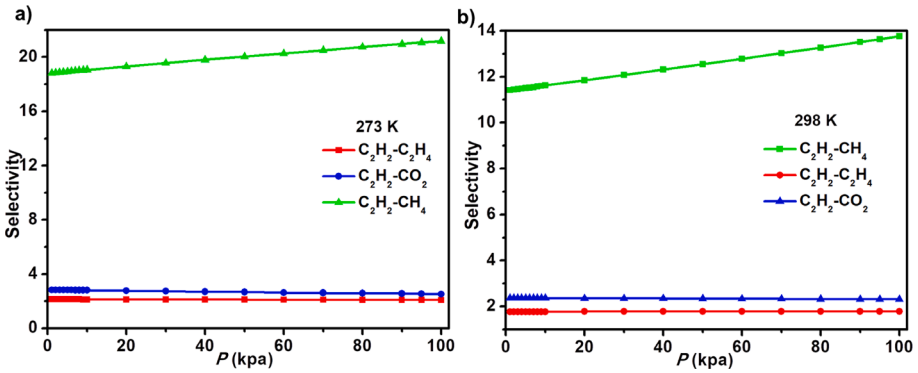

Fig. 3. a) and b) IAST predicted selectivities for equimolar C_2H_2-CO_2, C_2H_2-CH_4, and C_2H_2-C_2H_4 mixtures at 273 and 298 K.

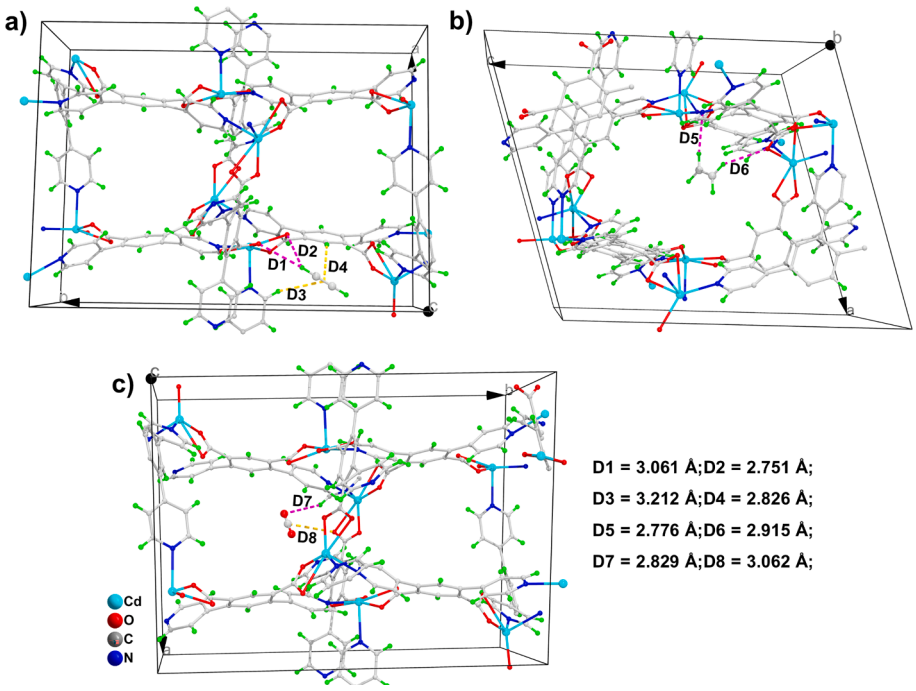

Fig. 4. Adsorption locus in **1a** for C_2H_2 (a), C_2H_4 (b), and CO_2 (c). (For interpretation of the references to colour in this figure legend, the reader is referred to the web version of this article.)

of **1a** (Fig. 2d). The adsorption enthalpy (Q_{st}) was used to evaluate the affinity of **1a** for gas molecules (Figure S8). A notable zero coverage Q_{st} value of **1a** for C_2H_2 (21.2 kJ mol^{-1}) that is higher than those of CH_4 (13.8 kJ mol^{-1}), C_2H_4 (18.8 kJ mol^{-1}), and CO_2 (19.6 kJ mol^{-1}) was indeed observed, illustrating the stronger affinity of **1a** for C_2H_2 than CH_4, C_2H_4, and CO_2 (Fig. 2e). Notably, the C_2H_2 Q_{st} value in **1a** is much lower than most MOF materials, such as Fe-MOF-74 [52], ATC-Cu [53], and TIFSIX-2-Cu-I [32], which indicate a less energy consume for C_2H_2 production (Fig. 2f and Table S4).

3.4. Gas selectivity

These differences in absorption uptakes and zero coverage Q_{st} for C_2H_2 and other gases indicate a promising material of **1a** for separating C_2H_2 from C_2H_2-containing mixtures. To evaluate the separation performance, the ideal adsorbed solution theory (IAST) method was

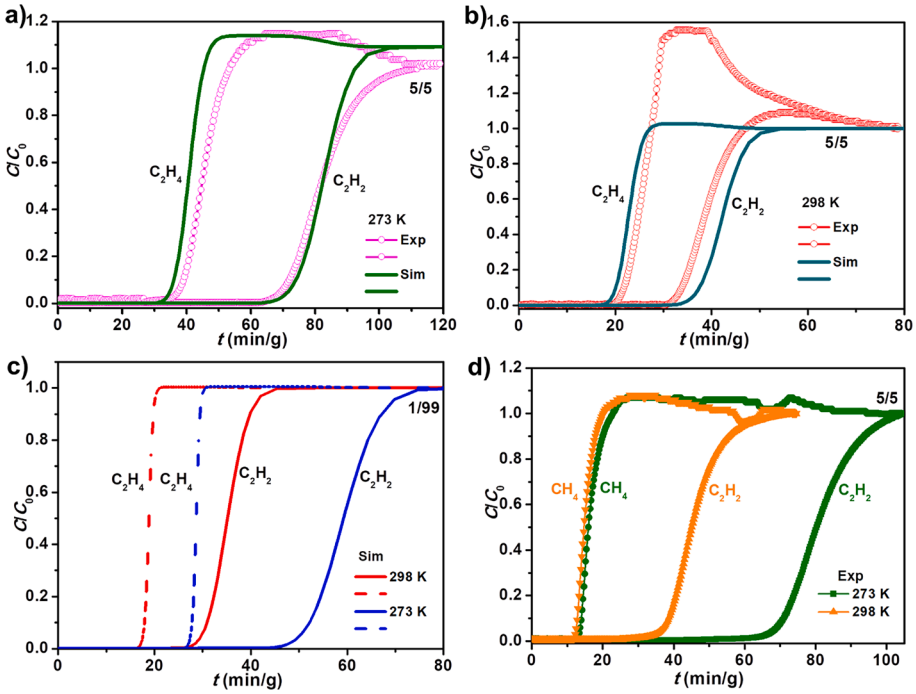

Fig. 5. a) and b) Comparison of the experimental and simulated breakthrough curves for C_2H_2/C_2H_4/Ar (5:5:90, v/v/v) separation at 273 and 298 K; c) simulated breakthrough curves for C_2H_2/C_2H_4 (1:99) separation at 273 and 298 K; d) experimental breakthrough curves for C_2H_2/CH_4/Ar (5:5:90, v/v/v) separation at 273 and 298 K.

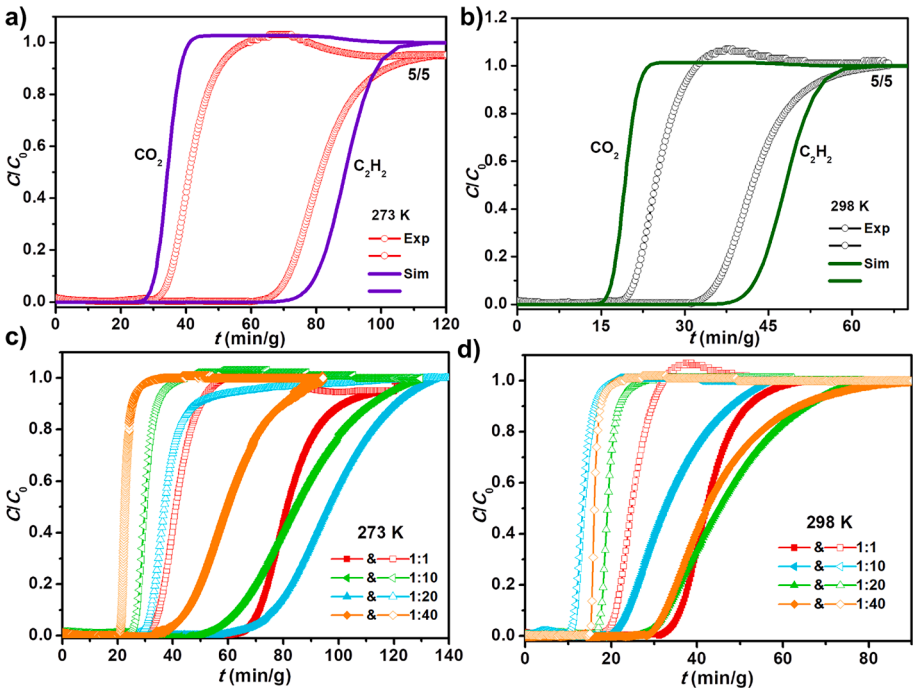

Fig. 6. a) and b) Comparison of experimental and simulated breakthrough curves for C_2H_2/CO_2/Ar (5:5:90, v/v/v) mixtures at 273 and 298 K; c) and d) breakthrough experiments for C_2H_2/CO_2 mixtures at different concentrations at 273 and 298 K.

employed to calculate the C_2H_2 selectivities through fitting sorption isotherms based on 1-site Langmuir model (Figure S9-S10). As depicted in Fig. 3a and 3b, the selectivities of equimolar C_2H_2-CH_4 for **1a** are 21.2 and 13.8 under 100 kPa at 273 and 298 K, respectively, which are comparable with [Ni(dpip)] (16.6) [54], SNNU-17 (20.3) [55], and ZJU-16a (17.7) [56]. The selectivities of equimolar C_2H_2-C_2H_4 and C_2H_2-CO_2 mixtures for **1a** are 2.1 and 1.8, and 2.5 and 2.3 under 100 kPa at 273 and 298 K, respectively. The C_2H_2/CO_2 selectivity value of 2.5 is better than the known materials M'MOF-2a (1.89) [57], Zn-MOF-74a (2) [49], and SNNU-27-Fe (2) [16]. The high C_2H_2 adsorption capacity and separation selectivity endow **1a** with the separation potential for C_2H_2-containing mixtures.

3.5. Molecular simulations

To in-depth understand the adsorption mechanism, Grand Canonical Monte Carlo simulations were conducted to explore the interplay among MOF and gas molecules. The calculated preferential adsorption locations for C_2H_2, C_2H_4, and CO_2 were shown in Fig. 4a-c. For C_2H_2 molecule, one –CH unit that lies close the accessible carboxyl O atoms of two independent ligands forms two C—H···O hydrogen bonds. Meantime, abundant π electron cloud of the triple bond group in C_2H_2 makes it form C—H···π contacts with the pyridine and benzene rings. Differently, C_2H_4 only forms one C—H···N and one C—H···O hydrogen bonds with the pyridine N atom and carboxyl O atom. For CO_2, its O and C atoms form one C—H···O and C···O interactions (C···O = 3.062 Å) with the –CH fragment in the pyridine ring and carboxyl O atom, respectively (Fig. 4c). In addition, the electrostatic potential (ESP) of **1a** mapped onto the Connolly surface results reveal that the negative potential regions of the triple bond group in C_2H_2 molecule is mainly stabilized by the attractive interactions with positive potential region near hydrogen atom of pyridine group (Figure S11). It is worth noting that since the open Cd^{2+} sites do not point into the channel, no M···π interaction is formed between the gas molecules and the framework, which is consistent with the low Q_{st} value observed experimentally. The simulations reveal the important dedication of the accessible adsorption locus including pyridine ring and carboxyl groups, which form multiform of supramolecular interactions between the framework and gas molecules. The more and stronger interactions for C_2H_2 lead to the most loading for C_2H_2 compared to CO_2 and C_2H_4.

3.6. Breakthrough separation

To validate the separation feasibility of **1a** in the packed column, transient breakthrough simulations for C_2H_2/C_2H_4/Ar (5:5:90, v/v/v) and C_2H_2/C_2H_4 (1/99, v/v) mixtures were done at 273/298 K under 100 kPa using the methodology described by Krishna (see also Supporting Information) [58,59]. The simulated curves in Fig. 5a,b display that the C_2H_2/C_2H_4 mixtures were efficiently separated by **1a**. The experimental breakthrough of gas mixtures (Ar as carrier gas) with a total rate of 5 mL min^{-1} flowed over a fixed-bed of **1a** sample at 298 and 273 K under 100 kPa were then tested. The experimental results were highly close to the simulated results at both temperatures; wherein C_2H_4 were first detected at the outlet while C_2H_2 was retained in bed for with longer times (Fig. 5a,b). And the time intervals are 11.4 and 28.6 min g^{-1} at 298 and 273 K, respectively. In addition, based on the experimental breakthrough curves, the amounts of C_2H_2 adsorbed by **1a** during the dynamic separation process can be calculated as 12.1 and 22.7 $cm^3\ g^{-1}$ from C_2H_2/C_2H_4 mixtures at 298 and 273 K. Furthermore, to thoroughly evaluate the desired target purity for C_2H_4 which contains less than about 40 ppm of C_2H_2 can be met with **1a**, we conducted more breakthrough simulations for 1/99 C_2H_2/C_2H_4 mixtures under 100 kPa pressure at 273 and 298 K (Fig. 5c). The productivities of ≥ 99.996% C_2H_4 purity were determined to be 27.72 and 60.77 L kg^{-1} in a single adsorption process, which are lower than the values of ZU-62-Ni (201.07 L kg^{-1}) [60], M'MOF-3a (144.52 L kg^{-1}) [61], UTSA-220 (75.24 L kg^{-1}) [62]. In addition, the experimental breakthrough of C_2H_2/CH_4/Ar (5:5:90, v/v/v) at 273 and 298 K were also conducted (Fig. 5d). The results display a highly efficient separation of C_2H_2 from the equimolar C_2H_2/CH_4 mixture can be realized by **1a** with the amounts of adsorbed C_2H_2 to be 12.5 and 22.2 $cm^3\ g^{-1}$ at 298 and 273 K, respectively.

Furthermore, breakthrough experiments were also implemented to validate the separation ability for C_2H_2/CO_2 mixtures. For the ratios of 1:1 mixture, Fig. 6a reveals that CO_2 breakthrough occurred

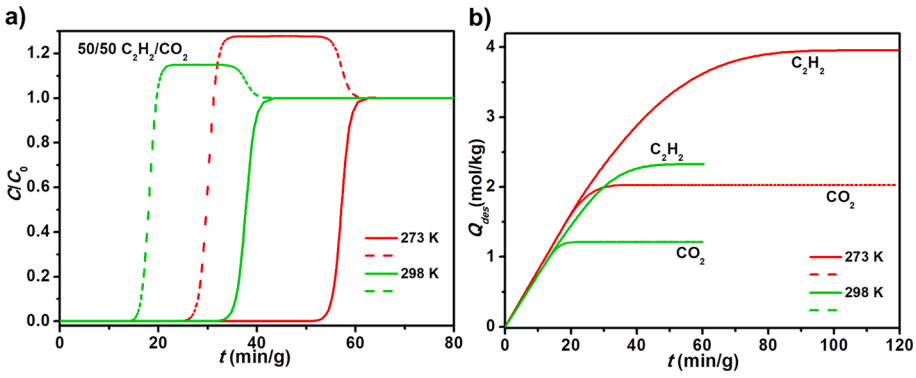

Fig. 7. a) Simulated breakthrough curves for 50/50 C_2H_2/CO_2 mixtures; b) cumulative moles of C_2H_2 and CO_2 recovered during blowdown.

significantly earlier in comparison to C_2H_2 (18.7 versus 32.6 min g^{-1} for 298 K and 31.5 versus 62.8 min g^{-1} for 273 K), revealing the stronger interactions between the framework and C_2H_2 molecules. During this process, the absorbed C_2H_2 amounts were calculated to be 22.4 and 13.2 cm^3 g^{-1} at 273 and 298 K, respectively, however, the co-adsorbed CO_2 amount were significantly low (11.1 and 6.5 cm^3 g^{-1}). On the basis of dynamic breakthrough experiments, the separation factor for **1a** reaches up to 2.0 at 273 and 298 K, which are comparable with the reports in best-performing FJU-6-TATB [50], FeNi-M'MOF [63], NKMOF-1-Ni [64], and FJU-90 [65]. For other ratios of C_2H_2-CO_2 mixtures (1:10, 1:20, and 1:40), **1a** also displays great separation ability (Fig. 6c and 6d). Cycling breakthrough experiments reveal the excellent reusability and regeneration of **1a**, which shows fully reproducible at least five consecutive adsorption–desorption runs through sweeping by Ar for 30 min at 313 K (Figure S12). In addition, the PXRD pattern and N_2 adsorption of the samples collected before and after the gas adsorption tests and breakthrough experiments are consistent (Figure S2 and Figure S13), verifying the framework stability.

Next, the transient breakthrough simulations for 50/50 C_2H_2/CO_2 mixtures for both the adsorption and desorption phase were also performed to validate the feasibility of **1a** for C_2H_2 purification from equimolar C_2H_2/CO_2 mixtures (Fig. 7a,b). The desorption cycle was simulated by applying deep vacuum as described by Wang et al [66]. The results in Fig. 7 show that **1a** can efficiently separate this mixtures with 2.32 and 3.95 mol kg^{-1} of C_2H_2 productivity at 298 and 273 K, respectively, which are comparable with the benchmark MOFs, such as ZNU-1 (2.9 mol kg^{-1} at 298 K) and BSF-3 (2.44 mol kg^{-1} at 298 K), and greatly exceeds the reported top-performance adsorbents, including DICRO-4-Cu-i (1.26 mol kg^{-1} at 298 K), MUF-17(1.79 mol kg^{-1} at 298 K), and BSF-1 (0.96 mol kg^{-1} at 298 K) [67].

4. Conclusions

In conclusion, a novel Cd-MOF was constructed by solvothermal method toward C_2H_2-related separation. The Cd-MOF features suitable pores surfaces modified by carboxylic acid oxygen atoms, affording ultrahigh C_2H_2 adsorption uptake of 124.4 cm^3 g^{-1}, which is significantly higher than C_2H_4 and CO_2 under ambient conditions. Breakthrough experiments confirm the effective separation of C_2H_2 from C_2H_2-C_2H_4, C_2H_2-CH_4, and C_2H_2-CO_2 mixtures by Cd-MOF. The simulated transient breakthroughs for 1/99 C_2H_2/C_2H_4 mixtures demonstrate that Cd-MOF can yield high-purity (>99.996%) C_2H_4 with high productivities of 27.72 at 298 K and 60.77 L kg^{-1} at 273 K. Furthermore, together with the low heat of adsorption (20.8 kJ mol^{-1}) and cycle tests of sorption isotherms and breakthrough curves, it indicates a low regeneration energy of Cd-MOF for during the process of C_2H_2 separation. This work provides a novel Cd-MOF to achieve excellent C_2H_2-related separation performance to push industrial implementation of MOF materials for some important gas separations.

CRediT authorship contribution statement

Yong-Zhi Li: Writing – original draft, Funding acquisition. **Rajamani Krishna:** Formal analysis, Software. **Fan Xu:** Formal analysis. **Wan-Fang Zhang:** Software. **Yanwei Sui:** Formal analysis, Funding acquisition. **Lei Hou:** Writing – review & editing, Supervision. **Yao-Yu Wang:** Formal analysis, Resources. **Zhonghua Zhu:** Formal analysis.

Declaration of Competing Interest

The authors declare that they have no known competing financial interests or personal relationships that could have appeared to influence the work reported in this paper.

Data availability

Data will be made available on request.

Acknowledgements

This work is supported by National Natural Science Foundation of China (No. 21871220), the Fundamental Research Funds for the Central Universities (No. 2022QN1089).

Appendix A. Supplementary data

Supplementary data to this article can be found online at https://doi.org/10.1016/j.seppur.2022.122678.

References

[1] D.S. Sholl, R.P. Lively, Seven chemical separations to change the world, Nature 532 (2016) 435.
[2] Q. Dong, Y. Huang, K. Hyeon-Deuk, I.-Y. Chang, J. Wan, C. Chen, J. Duan, W. Jin, S. Kitagawa, Shape- and Size-Dependent Kinetic Ethylene Sieving from a Ternary Mixture by a Trap-and-Flow Channel Crystal, Adv. Funct. Mater. 2203745 (2022).
[3] P. Zhang, Y. Zhong, Y. Zhang, Z. Zhu, Y. Liu, Y. Su, J. Chen, S. Chen, Z. Zeng, H. Xing, S. Deng, J. Wang, Synergistic binding sites in a hybrid ultramicroporous material for one-step ethylene purification from ternary C_2 hydrocarbon mixtures, Sci. Adv. 8 (2022) eabn9231.
[4] Q. Zhang, L. Zhou, P. Liu, L. Li, S.-Q. Yang, Z.-F. Li, T.-L. Hu, Integrating tri-mural nanotraps into a microporous metal-organic framework for C_2H_2/CO_2 and C_2H_2/C_2H_4 separation, Sep. Purif. Technol. 296 (2022), 121404.
[5] J. Pei, K. Shao, J.-X. Wang, H.-M. Wen, Y. Yang, Y. Cui, R. Krishna, B. Li, G. Qian, A Chemically Stable Hofmann-Type Metal-Organic Framework with Sandwich-Like Binding Sites for Benchmark Acetylene Capture, Adv. Mater. 32 (2020) 1908275.
[6] X.-P. Fu, Y.-L. Wang, X.-F. Zhang, R. Krishna, C.-T. He, Q.-Y. Liu, B. Chen, Collaborative pore partition and pore surface fluorination within a metal-organic framework for high-performance C_2H_2/CO_2 separation, Chem. Eng. J. 432 (2022), 134433.
[7] Y.-M. Gu, H.-F. Qi, T.-T. Sun, X.-W. Liu, S. Qadir, T.-J. Sun, D.-F. Li, S.-S. Zhao, D. Fairen-Jimenez, S.-D. Wang, Insights into the Ultra-High Volumetric Capacity in a Robust Metal-Organic Framework for Efficient C_2H_2/CO_2 Separation, Chem. Mater. 34 (2022) 2708–2716.

[8] X.-J. Xie, H. Zeng, M. Xie, W. Chen, G.-F. Hua, W. Lu, D. Li, A metal-organic framework for C_2H_2/CO_2 separation under highly humid conditions: Balanced hydrophilicity/hydrophobicity, Chem. Eng. J. 427 (2022), 132033.
[9] H.-P. Li, Z.-D. Dou, Y. Wang, Y.Y. Xue, Y.P. Li, M.-C. Hu, S.-N. Li, Y.-C. Jiang, Q.-G. Zhai, Tuning the Pore Surface of an Ultramicroporous Framework for Enhanced Methane and Acetylene Purification Performance, Inorg. Chem. 59 (2020) 16725–16736.
[10] X. Cui, K. Chen, H. Xing, Q. Yang, R. Krishna, Z. Bao, H. Wu, W. Zhou, X. Dong, Y. Han, B. Li, Q. Ren, M.J. Zaworotko, B. Chen, Pore chemistry and size control in hybrid porous materials for acetylene capture from ethylene, Science 353 (2016) 141–144.
[11] W. Sun, J. Hu, S. Duttwyler, L. Wang, R. Krishna, Y. Zhang, Highly selective gas separation by two isostructural boron cluster pillared MOFs, Sep. Purif. Technol. 283 (2022), 120220.
[12] Y. Zhao, J. Wang, Z. Bao, H. Xing, Z. Zhang, B. Su, Q. Yang, Y. Yang, Q. Ren, Adsorption separation of acetylene and ethylene in a highly thermostable microporous metal-organic framework, Sep. Purif. Technol. 195 (2018) 238–243.
[13] J.-R. Li, R.J. Kupplera, H.-C. Zhou, Selective gas adsorption and separation in metal-organic frameworks, Chem. Soc. Rev. 38 (2009) 1477–1504.
[14] Y. Wang, C. Hao, W. Fan, M. Fu, X. Wang, Z. Wang, L. Zhu, Y. Li, X. Lu, F. Dai, Z. Kang, R. Wang, W. Guo, S. Hu, D. Sun, One-step Ethylene Purification from an Acetylene/Ethylene/Ethane Ternary Mixture by Cyclopentadiene Cobalt-Functionalized Metal-Organic Frameworks, Angew. Chem. Int. Ed. 60 (2021) 11350–11358.
[15] K.-J. Chen, D.G. Madden, S. Mukherjee, T. Pham, K.A. Forrest, A. Kumar, B. Space, J. Kong, Q.-Y. Zhang, M.J. Zaworotko, Synergistic sorbent separation for one-step ethylene purification from a four-component mixture, Science 366 (2019) 241–246.
[16] Y.-Y. Xue, X.-Y. Bai, J. Zhang, Y. Wang, S.-N. Li, Y.-C. Jiang, M.-C. Hu, Q.-G. Zhai, Precise Pore Space Partition Combined with High-Density Hydrogen-Bonding Acceptor within a Metal-Organic Framework for Highly Efficient Acetylene Storage and Separation, Angew. Chem. Int. Ed. 60 (2021) 10122–10128.
[17] X.-R. Tian, X.-L. Jiang, S.-L. Hou, Z.-H. Jiao, J. Han, B. Zhao, Selectively Regulating Lewis Acid-Base Sites in Metal-Organic Frameworks for Achieving Turn-On/Off of the Catalytic Activity in Different CO_2 Reactions, Angew. Chem. Int. Ed. 61 (2022) e202200123.
[18] S.-Q. Yang, T.-L. Hu, Reverse-selective metal-organic framework materials for the efficient separation and purification of light hydrocarbons, Coord. Chem. Rev. 468 (2022), 214628.
[19] J.-B. Lin, T.T.T. Nguyen, R. Vaidhyanathan, J. Burner, J.M. Taylor, H. Durekova, F. Akhtar, R.K. Mah, O. Ghaffari-Nik, S. Marx, N. Fylstra, S.S. Iremonger, K. W. Dawson, P. Sarkar, P. Hovington, A. Rajendran, T.K. Woo, G.K.H. Shimizu, A scalable metal-organic framework as a durable physisorbent for carbon dioxide capture, Science 374 (2021) 1464–1469.
[20] S. Zhou, O. Shekhah, A. Ramírez, P. Lyu, E. Abou-Hamad, J. Jia, J. Li, P.M. Bhatt, Z. Huang, H. Jiang, T. Jin, G. Maurin, J. Gascon, M. Eddaoudi, Asymmetric pore windows in MOF membranes for natural gas valorization, Nature 606 (2022) 706–712.
[21] J. Zhao, Z.-H. Jiao, S.-L. Hou, Y. Ma, B. Zhao, Anchoring Ag(I) into Nitro-Functionalized Metal-Organic Frameworks: Effectively Catalyzing Cycloaddition of CO_2 with Propargylic Alcohols under Mild Conditions, ACS Appl. Mater. Interfaces 13 (2021) 45558–45565.
[22] M.A. Lemes, N. Mavragani, P. Richardson, Y. Zhang, B. Gabidullin, J.L. Brusso, J. O. Moilanen, M. Murugesu, Unprecedented intramolecular pancake bonding in a Dy2 single-molecule magnet, Inorg. Chem. Front. 7 (2020) 2592–2601.
[23] Y. Sun, B. Bao, Y. Zhu, J. Shen, X. Liu, T. Gao, J. Lin, T. Huang, J. Xu, Y. Chai, X. Zheng, An FPS-ZM1-encapsulated zeolitic imidazolate framework as a dual proangiogenic drug delivery system for diabetic wound healing, Nano Res. 15 (2022) 5216–5229.
[24] Y. Yoshida, T. Yamada, Y. Jing, T. Toyao, K. Shimizu, M. Sadakiyo, Super Mg^{2+} Conductivity around 10^{-3} S cm^{-1} Observed in a Porous Metal-Organic Framework, J. Am. Chem. Soc. 144 (2022) 8669–8675.
[25] H. Zeng, M. Xie, T. Wang, R.-J. Wei, X.-J. Xie, Y. Zhao, W. Lu, D. Li, Orthogonal-array dynamic molecular sieving of propylene/propane mixtures, Nature 595 (2022) 542–548.
[26] P.-Q. Liao, N.-Y. Huang, W.-X. Zhang, J.-P. Zhang, X.-M. Chen, Controlling guest conformation for efficient purification of butadiene, Science 356 (2017) 1193–1196.
[27] G.-D. Wang, Y.-Z. Li, W.-J. Shi, L. Hou, Y.-Y. Wang, Z. Zhu, One-Step C_2H_4 Purification from Ternary $C_2H_6/C_2H_4/C_2H_2$ Mixtures by a Robust Metal-Organic Framework with Customized Pore Environment, Angew. Chem. Int. Ed. 61 (2022) e202205427.
[28] B.-Y. Zhu, T. Zhang, C.-H. Li, J.-W. Cao, Z.-Q. Zhang, W. Qi, G.-Y. Wang, Z.-H. Rong, Y. Wang, K.-J. Chen, A (3,8)-Connected Metal-Organic Framework with Bending Dicarboxylate Linkers for C_2H_2/CO_2 Separation, Inorg. Chem. 61 (2022) 4555–4560.
[29] J. Pei, H.-M. Wen, X.-W. Gu, Q.-L. Qian, Y. Yang, Y. Cui, B. Li, B. Chen, G. Qian, Dense Packing of Acetylene in a Stable and Low-Cost Metal-Organic Framework for Efficient C_2H_2/CO_2 Separation, Angew. Chem. Int. Ed. 60 (2021) 25068–25074.
[30] G.-D. Wang, R. Krishna, Y.-Z. Li, W.-J. Shi, L. Hou, Y.-Y. Wang, Z. Zhu, Boosting Ethane/Ethylene Separation by MOFs through the Amino-Functionalization of Pores, Angew. Chem. Int. Ed. (2022) e202213015.
[31] D. Luo, Y.-L. Peng, M. Xie, M. Li, A.A. Bezrukov, T. Zuo, X.-Z. Wang, Y. Wu, Y.Y. Li, A.R. Lowe, M. Chorążewski, Y. Grosu, Z. Zhang, M.J. Zaworotko, X.-P. Zhou, D. Li, Improving Ethane/Ethylene Separation Performance under Humid Conditions by Spatially Modified Zeolitic Imidazolate Frameworks, ACS Appl. Mater. Interfaces 14 (2022) 11547–11558.
[32] K.-J. Chen, H.S. Scott, D.G. Madden, T. Pham, A. Kumar, A. Bajpai, M. Lusi, K. A. Forrest, B. Space, J.J. Perry IV, M.J. Zaworotko, Benchmark C_2H_2/CO_2 and CO_2/C_2H_2 Separation by Two Closely Related Hybrid Ultramicroporous Materials, Chem. 1 (2016) 753–765.
[33] B. Liang, X. Zhang, Y. Xie, R.-B. Lin, R. Krishna, H. Cui, Z. Li, Y. Shi, H. Wu, W. Zhou, B. Chen, An Ultramicroporous Metal-Organic Framework for High Sieving Separation of Propylene from Propane, J. Am. Chem. Soc. 142 (2020) 17795–17801.
[34] H. Wang, Y. Liu, J. Li, Designer Metal-Organic Frameworks for Size-Exclusion-Based Hydrocarbon Separations: Progress and Challenges, Adv. Mater. 32 (2020) 2002603.
[35] Z. Di, C. Liu, J. Pang, C. Chen, F. Hu, D. Yuan, M. Wu, M. Hong, Cage-like Porous Materials with Simultaneous High C_2H_2 Storage and Excellent C_2H_2/CO_2 Separation Performance, Angew. Chem. Int. Ed. 60 (2021) 10828–10832.
[36] L. Zhang, K. Jiang, L. Yang, L. Li, E. Hu, L. Yang, K. Shao, H. Xing, Y. Cui, Y. Yang, B. Li, B. Chen, G. Qian, Benchmark C_2H_2/CO_2 Separation in an Ultramicroporous Metal-Organic Framework via Copper(I) Alkynyl Chemistry, Angew. Chem. Int. Ed. 60 (2021) 15995–16002.
[37] S. Sharma, S. Mukherjee, A.V. Desai, M. Vandichel, G.K. Dam, A. Jadhav, G. Kociok-Köhn, M.J. Zaworotko, S.K. Ghosh, Efficient Capture of Trace Acetylene by an Ultramicroporous Metal-Organic Framework with Purine Binding Sites, Chem. Mater. 33 (2021) 5800–5808.
[38] W. Fan, S. Yuan, W. Wang, L. Feng, X. Liu, X. Zhang, X. Wang, Z. Kang, F. Dai, D. Yuan, D. Sun, H.-C. Zhou, Optimizing Multivariate Metal-Organic Frameworks for Efficient C_2H_2/CO_2 Separation, J. Am. Chem. Soc. 142 (2020) 8728–8737.
[39] W. Fan, S.B. Peh, Z. Zhang, H. Yuan, Z. Yang, Y. Wang, K. Chai, D. Sun, D. Zhao, Tetrazole-Functionalized Zirconium Metal-Organic Cages for Efficient C_2H_2/C_2H_4 and C_2H_2/CO_2 Separations, Angew. Chem. Int. Ed. 60 (2021) 17338–17343.
[40] L. Sarkisov, R. Bueno-Perez, M. Sutharson, D. Fairen-Jimenez, Materials Informatics with PoreBlazer v4.0 and the CSD MOF Database, Chem. Mater. 32 (2020) 9849–9867.
[41] B. Wang, X.-L. Lv, D. Feng, L.-H. Xie, J. Zhang, M. Li, Y. Xie, J.-R. Li, H.-C. Zhou, Highly Stable Zr(IV)-Based Metal-Organic Frameworks for the Detection and Removal of Antibiotics and Organic Explosives in Water, J. Am. Chem. Soc. 138 (2016) 6204–6216.
[42] Z. Xu, X. Xiong, J. Xiong, R. Krishna, L. Li, Y. Fan, F. Luo, B. Chen, A robust Th-azole framework for highly efficient purification of C_2H_4 from a $C_2H_4/C_2H_2/C_2H_6$ mixture, Nat. Commun. 11 (2020) 3163.
[43] Y. Ye, S. Xian, H. Cui, K. Tan, L. Gong, B. Liang, T. Pham, H. Pandey, R. Krishna, P. C. Lan, K.A. Forrest, B. Space, T. Thonhauser, J. Li, S. Ma, Metal-Organic Framework Based Hydrogen-Bonding Nanotrap for Efficient Acetylene Storage and Separation, J. Am. Chem. Soc. 144 (2022) 1681–1689.
[44] S. Xiang, W. Zhou, J.M. Gallegos, Y. Liu, B. Chen, Exceptionally High Acetylene Uptake in a Microporous Metal-Organic Framework with Open Metal Sites, J. Am. Chem. Soc. 131 (2009) 12415–12419.
[45] S.-Q. Yang, F.-Z. Sun, P. Liu, L. Li, R. Krishna, Y.-H. Zhang, Q. Li, L. Zhou, T.-L. Hu, Efficient Purification of Ethylene from C_2 Hydrocarbons with an $_C2_H6/_C2_H2$-Selective Metal-Organic Framework, ACS Appl. Mater. Interfaces 13 (2021) 962–969.
[46] T.-L. Hu, H. Wang, B. Li, R. Krishna, H. Wu, W. Zhou, Y. Zhao, Y. Han, X. Wang, W. Zhu, Z. Yao, S. Xiang, B. Chen, Microporous metal-organic framework with dual functionalities for highly efficient removal of acetylene from ethylene/acetylene mixtures, Nat. Commun. 6 (2015) 7328.
[47] B. Zhu, J.-W. Cao, S. Mukherjee, T. Pham, T. Zhang, T. Wang, X. Jiang, K. A. Forrest, M.J. Zaworotko, K.-J. Chen, Pore Engineering for One-Step Ethylene Purification from a Three-Component Hydrocarbon Mixture, J. Am. Chem. Soc. 143 (2021) 1485–1492.
[48] X. Zhang, W. Fan, W. Jiang, Y. Li, Y. Wang, M. Fu, D. Sun, Optimizing Fe-Based Metal-Organic Frameworks through Ligand Conformation Regulation for Efficient Dye Adsorption and C_2H_2/CO_2 Separation, Chem. Eur. J. 27 (2021) 10693–10699.
[49] F. Luo, C. Yan, L. Dang, R. Krishna, W. Zhou, H. Wu, X. Dong, Y. Han, T.-L. Hu, M. O'Keeffe, L. Wang, M. Luo, R.-B. Lin, B. Chen, UTSA-74: A MOF-74 Isomer with Two Accessible Binding Sites per Metal Center for Highly Selective Gas Separation, J. Am. Chem. Soc. 138 (2016) 5678–5684.
[50] L. Liu, Z. Yao, Y. Ye, Y. Yang, Q. Lin, Z. Zhang, M. O'Keeffe, S. Xiang, Integrating the Pillared-Layer Strategy and Pore-Space Partition Method to Construct Multicomponent MOFs for C_2H_2/CO_2 Separation, J. Am. Chem. Soc. 142 (2020) 9258–9266.
[51] G.-D. Wang, H.-H. Wang, W.-J. Shi, L. Hou, Y.-Y. Wang, Z. Zhu, A highly stable MOF with F and N accessible sites for efficient capture and separation of acetylene from ternary mixtures, J. Mater. Chem. A 9 (2021) 24495–24502.
[52] E.D. Bloch, W.L. Queen, R. Krishna, J.M. Zadrozny, C.M. Brown, J.R. Long, Hydrocarbon Separations in a Metal-Organic Framework with Open Iron(II) Coordination Sites, Science 335 (2012) 1606–1610.
[53] Z. Niu, X. Cui, T. Pham, G. Verma, P.C. Lan, C. Shan, H. Xing, K.A. Forrest, S. Suepaul, B. Space, A. Nafady, A.M. Al-Enizi, S. Ma, A MOF-based Ultra-Strong Acetylene Nano-trap for Highly Efficient C_2H_2/CO_2 Separation, Angew. Chem. Int. Ed. 60 (2021) 5283–5288.
[54] Y.-Z. Li, G.-D. Wang, L.-N. Ma, L. Hou, Y.-Y. Wang, Z. Zhu, Multiple Functions of Gas Separation and Vapor Adsorption in a New MOF with Open Tubular Channels, ACS Appl. Mater. Interfaces 13 (2021) 4102–4109.
[55] H.-P. Li, Y.-Y. Xue, Y. Wang, H. Sun, M.-C. Hu, S.-N. Li, Y. Jiang, Q.-G. Zhai, Regulation on Topological Architectures and Gas Adsorption for Cadmium-Azolate-

Carboxylate Frameworks by the Ligand Flexibility, Cryst. Growth Des. 21 (2021) 1718–1726.
[56] L. Liu, Z. Yao, Y. Ye, L. Chen, Q. Lin, Y. Yang, Z. Zhang, S. Xiang, Robustness, Selective Gas Separation, and Nitrobenzene Sensing on Two Isomers of Cadmium Metal-Organic Frameworks Containing Various Metal-O-Metal Chains, Inorg. Chem. 57 (2018) 12961–12968.
[57] S.-C. Xiang, Z. Zhang, C.-G. Zhao, K. Hong, X. Zhao, D.-R. Ding, M.-H. Xie, C.-D. Wu, M.C. Das, R. Gill, K.M. Thomas, B. Chen, Rationally tuned micropores within enantiopure metal-organic frameworks for highly selective separation of acetylene and ethylene, Nat. Commun. 2 (2011) 204.
[58] R. Krishna, Metrics for Evaluation and Screening of Metal-Organic Frameworks for Applications in Mixture Separations, ACS Omega 5 (2020) 16987–17004.
[59] R. Krishna, Screening Metal-Organic Frameworks for Mixture Separations in Fixed-Bed Adsorbers using a Combined Selectivity/Capacity Metric, RSC Adv. 7 (2017) 35724–35737.
[60] L. Yang, A. Jin, L. Ge, X. Cui, H. Xing, A novel interpenetrated anion-pillared porous material with high water tolerance afforded efficient C_2H_2/C_2H_4 separation, Chem. Commun. 55 (2019) 5001–5004.
[61] H.-H. Wang, Q.-Y. Liu, L. Li, R. Krishna, Y.-L. Wang, X.-W. Peng, C.-T. He, R.-B. Lin, B. Chen, Nickel-4'-(3,5-dicarboxyphenyl)-2,2',6',2"-terpyridine Framework: Efficient Separation of Ethylene from Acetylene/Ethylene Mixtures with a High Productivity, Inorg. Chem. 57 (2018) 9489–9494.
[62] H. Li, L. Li, R.-B. Lin, G. Ramirez, W. Zhou, R. Krishna, Z. Zhang, S. Xiang, B. Chen, Microporous Metal-Organic Framework with Dual Functionalities for Efficient Separation of Acetylene from Light Hydrocarbon Mixtures, ACS Sustainable Chem. Eng. 7 (2019) 4897–4902.
[63] J. Gao, X. Qian, R.-B. Lin, R. Krishna, H. Wu, W. Zhou, B. Chen, Mixed Metal-Organic Framework with Multiple Binding Sites for Efficient C_2H_2/CO_2 Separation, Angew. Chem. Int. Ed. 59 (2020) 4396–4400.
[64] Y.-L. Peng, T. Pham, P. Li, T. Wang, Y. Chen, K.-J. Chen, K.A. Forrest, B. Space, P. Cheng, M.J. Zaworotko, Z. Zhang, Robust Ultramicroporous Metal-Organic Frameworks with Benchmark Affinity for Acetylene, Angew. Chem., Int. Ed. 57 (2018) 10971–10975.
[65] Y. Ye, Z. Ma, R.-B. Lin, R. Krishna, W. Zhou, Q. Lin, Z. Zhang, S. Xiang, B. Chen, Pore Space Partition within a Metal-Organic Framework for Highly Efficient C_2H_2/CO_2 Separation, J. Am. Chem. Soc. 141 (2019) 4130–4136.
[66] L. Wang, W. Sun, Y. Zhang, N. Xu, R. Krishna, J. Hu, Y. Jiang, Y. He, H. Xing, Interpenetration symmetry control within ultramicroporous robust boron cluster hybrid MOFs for benchmark purification of acetylene from carbon dioxide, Angew. Chem. Int. Ed. 60 (2021) 22865–22870.
[67] Y. Zhang, J. Hu, R. Krishna, L. Wang, L. Yang, X. Cui, S. Duttwyler, H. Xing, Rational Design of Microporous MOFs with Anionic Boron Cluster Functionality and Cooperative Dihydrogen Binding Sites for Highly Selective Capture of Acetylene, Angew. Chem. Int. Ed. 59 (2020) 17664–17669.

Supporting Information

A novel C_2H_2-selective microporous Cd-MOF for C_2H_2/C_2H_4 and C_2H_2/CO_2 separation

Yong-Zhi Li,[a] Rajamani Krishna,[c] Fan Xu,[a] Wan-Fang Zhang,[b] Yanwei Sui,[a] Lei Hou,*[,b] Yao-Yu Wang[b] and Zhonghua Zhu[d]

[a] School of Materials and Physics, China University of Mining and Technology, Xuzhou 221116, P. R. China

[b] Key Laboratory of Synthetic and Natural Functional Molecule of the Ministry of Education, Shaanxi Key Laboratory of Physico-Inorganic Chemistry, College of Chemistry & Materials Science, Northwest University, Xi'an 710069, P. R. China.

[c] Van 't Hoff Institute for Molecular Sciences, University of Amsterdam, 1098 XH Amsterdam, The Netherlands.

[d] School of Chemical Engineering, The University of Queensland, Brisbane 4072, Australia.

* To whom correspondence should be addressed. E-mail: lhou2009@nwu.edu.cn (Lei Hou).

X-Ray Crystallography

A Bruker Smart Apex II CCD detector was used to collect the single crystal data at 189(2) K using Mo Kα radiation (λ = 0.71073 Å). The structure was solved by direct methods and refined by full-matrix least-squares refinement based on F^2 with the SHELXTL program.The non-hydrogen atoms were refined anisotropically with the hydrogen atoms added at their geometrically ideal positions and refined isotropically. As the disordered solvent H_2O molecules in the structure cannot be located, the SQUEEZE routine of Platon program was applied in refining. The formula of complex was got by the single crystal analysis together with elemental microanalyses and TGA data. Relevant crystallographic results are listed in Table S1. Selected bond lengths and angles are provided in Table S2.

N_2 Sorption Isotherm

Before gas sorption experiments, All the as-synthesized samples were immersed in CH_2Cl_2 for 3 days, during which the solvent was decanted and freshly replenished three times a day. All the samples were activated under vacuum at 423 K for 4 hours. Gas sorption measurements were then conducted using a Micrometrics ASAP 2020M gas adsorption analyzer.

Breakthrough Experiments

The breakthrough experiment was performed on the Quantachrome dynaSorb BT equipments at 298 K and 1 bar with an equal volume of mixed gas (gas A: gas B: Ar = 5% : 5% : 90%, Ar as the carrier gas, flow rate = 5 mL min^{-1}). The activated **1a** (0.85 g) was filled into a packed column of 4.2×80 mm, and then the packed column was washed with Ar at a rate of 7 mL min^{-1} at 353 K for 35 minutes to further activate the samples. Between two breakthrough experiments, the adsorbent was regenerated by Ar flow of 7 mL min^{-1} for 35 min at 353 K to guarantee a complete removal of the adsorbed gases.

GCMC Simulation

Grand canonical Monte Carlo (GCMC) simulations were performed for the gas adsorption in the framework by the Sorption module of Material Studio (Accelrys. Materials Studio Getting Started, release 5.0). The framework was considered to be rigid, and the optimized gases were used. The atom charges and bond lengths for the gas molecules are as follows:

CO_2, C = 0.576000e, O = -0.288000e, C-O = 1.168 Å.

C_2H_2, C = -0.238847 e, H = 0.238847 e, C-C = 1.198 Å, C-H = 1.065 Å.

C_2H_4, C = -0.295071 e, H = 0.147536 e, C-C = 1.334 Å, C-H = 1.090 Å.

The partial charges for atoms of the framework were derived from QEq method and QEq neutral 1.0 parameter. One unit cell was used during the simulations. The interaction energies between the gas molecules and framework were computed through the Coulomb and Lennard-Jones 6-12 (LJ) potentials. All parameters for the atoms were modeled with the universal force field (UFF) embedded in the MS modeling package. A cutoff distance of 12.5 Å was used for LJ interactions, and the Coulombic interactions were calculated by using Ewald summation. For each run, the 3×10^6 maximum loading steps, 3×10^6 production steps were employed.

Fitting Adsorption Heat of Pure Component Isotherms

$$\ln P = \ln N + 1/T\sum_{i=0}^{m} a_i N^i + \sum_{i=0}^{n} b_i N^i \qquad Q_{st} = -R\sum_{i=0}^{m} a_i N^i$$

The above virial expression was used to fit the combined isotherm data for **1a** at 273.15 and 298 K, where P is the pressure, N is the adsorbed amount, T is the temperature, a_i and b_i are virial coefficients, and m and N are the number of coefficients used to describe the isotherms. Q_{st} is the coverage-dependent enthalpy of adsorption and R is the universal gas constant.

Gas Selectivity Prediction via IAST

The experimental isotherm data for pure C_2H_2, C_2H_4, CO_2 and CH_4 were fitted using a single-site Langmuir equation model:

$$\boldsymbol{q} = \mathrm{a}\frac{b*p^{1-c}}{1+b*p^{1-c}}$$

Where q and p are adsorbed amounts and the pressure of component i, respectively.

The adsorption selectivities for binary mixtures of C_2H_2/C_2H_4, C_2H_2/CO_2 and C_2H_2/CH_4, defined by

$$S_{i/j} = \frac{x_i * y_j}{x_j * y_i}$$

were respectively calculated using the Ideal Adsorption Solution Theory (IAST). Where x_i is

the mole fraction of component i in the adsorbed phase and y_i is the mole fraction of component i in the bulk.

Transient breakthrough simulations

Transient breakthrough simulations were carried out for the same set of operating conditions as in the experimental data sets, using the methodology described in earlier publications.[S1-S5] Breakthrough simulations were conducted for the following set of conditions. In these simulations, intra-crystalline diffusion influences are ignored. In all the simulations: length of packed bed, L = 8 cm; inner diameter of packed bed, d = 4.2 mm; mass of **1a** = 0.41 g; framework density for **1a** = 0.89 g cm^{-3}; total volumetric flow rate of gas mixture at inlet = 5.0 mL min^{-1} (298 K and 273 K, 100 kPa).

Breakthrough simulations were also performed for 1/99 C_2H_2/C_2H_4 mixtures at 100 kPa total pressure (without inert Ar); the productivities of 99.996% pure C_2H_4 were determined; these are expressed in the units of L per kg of MOF.

Breakthrough simulations were also performed for 50/50 C_2H_2/CO_2 mixtures (without inert Ar) for both the adsorption and desorption phase. The desorption cycle was simulated by applying deep vacuum as described by Wang et al.[S6] The desorption cycle is initiated just before C_2H_2 breaks through in the adsorption cycle.

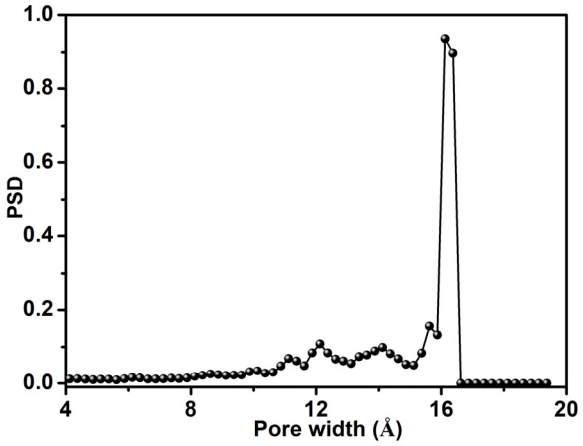

Figure S1. Pore distribution curve calculated from poreblazer software

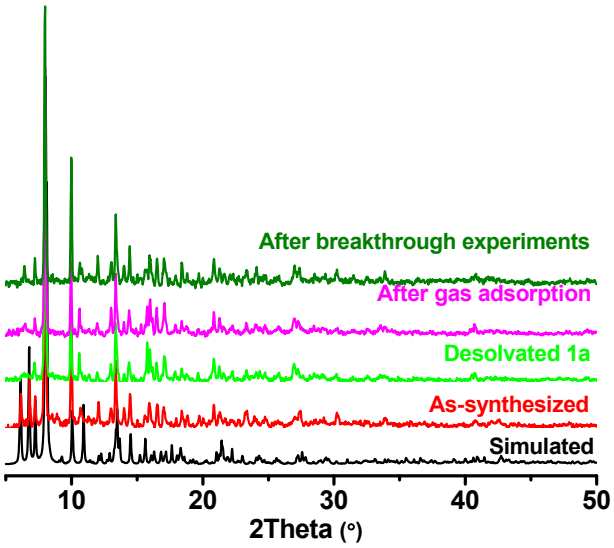

Figure S2. PXRD patterns of complex **1**.

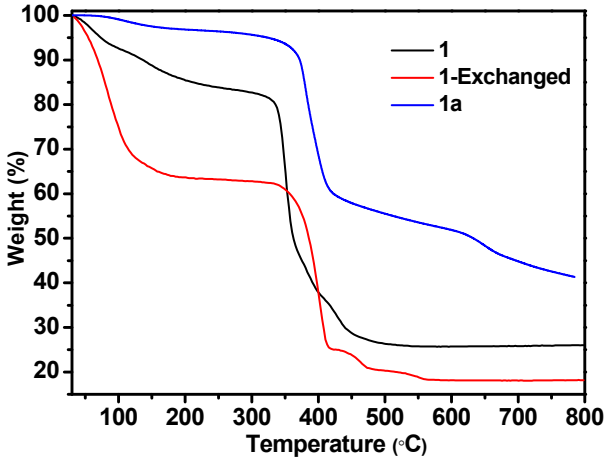

Figure S3. TGA curves of as-synthesized, CH_2Cl_2-exchanged and activated samples of complex **1**.

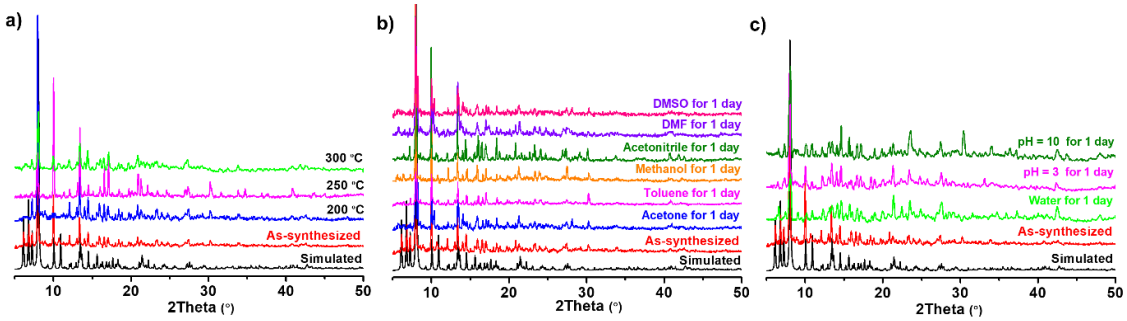

Figure S4. PXRD patterns of **1** after different treatments: a) heated at different temperatures;

b) soaked in organic solvents; c) water tolerability experiments.

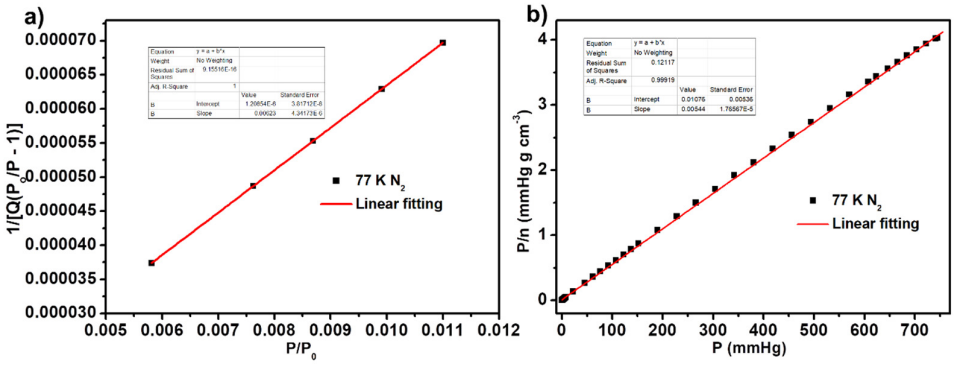

S_{BET} = 1/(1.20854×10^{-6} +0.00623)/22414 × 6.023 × 10^{23} × 0.162 × 10^{-18} =698 m^2 g^{-1}

$S_{Langmuir}$ = (1/0.00544)/22414 × 6.023 × 10^{23} × 0.162 × 10^{-18} = 800 m^2 g^{-1}

Figure S5. a) BET surface area plot and b) Langmuir surface area plot for **1a**.

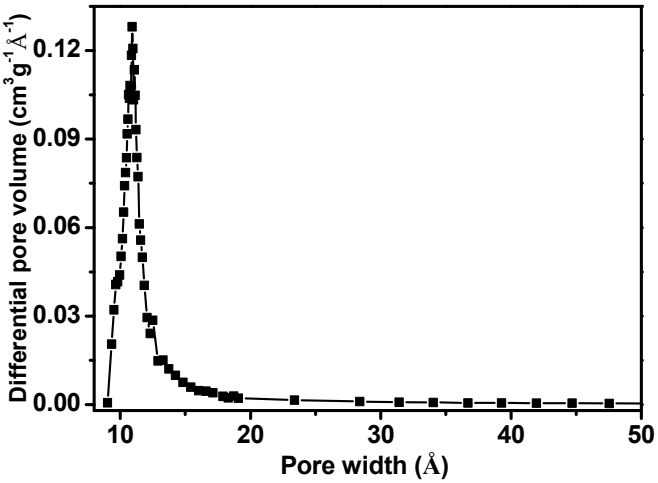

Figure S6. Pore distribution curve calculated from the N_2 adsorption isotherm at 77 K for **1a** using the Horvath-Kawazoe model.

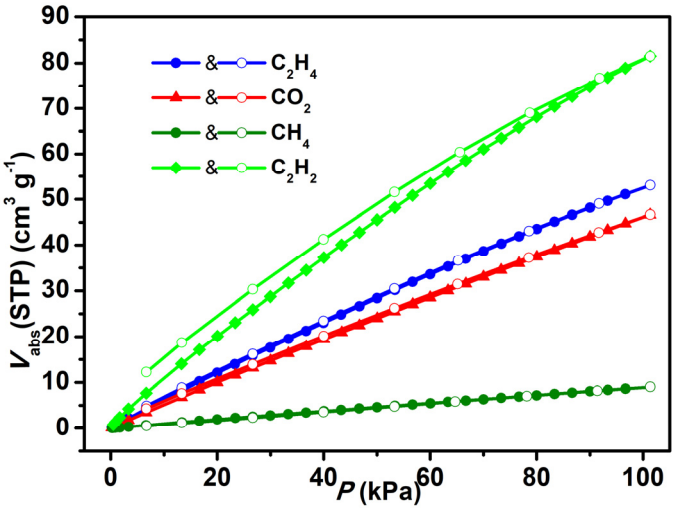

Figure S7. C_2H_2, C_2H_4, CO_2 and CH_4 adsorption isotherms of **1a** at 313 K

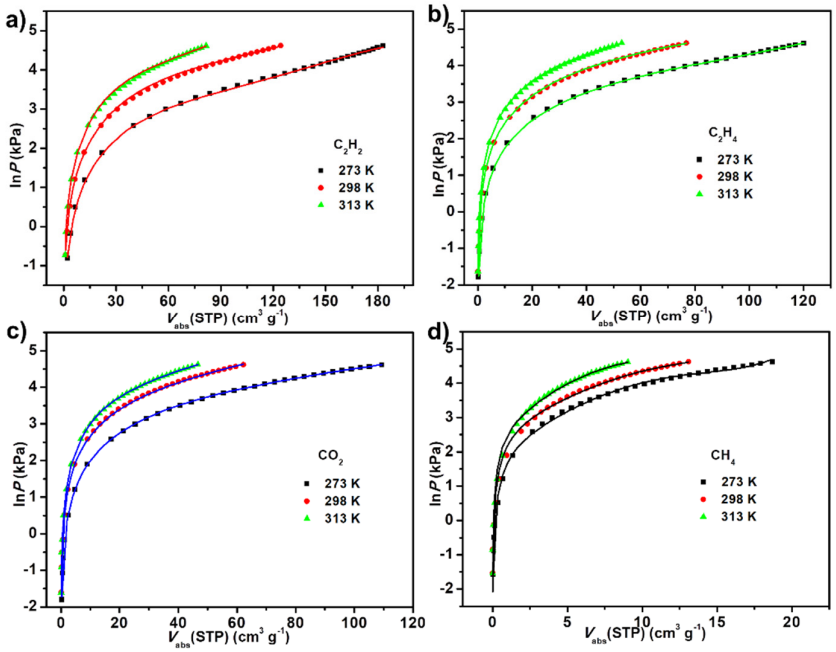

Viral Coefficient	C_2H_2 Value	C_2H_4 Value	CO_2 Value	CH_4 Value
a0	-2551.31286	-2267.46136	-2361.92993	-1658.8596
a1	1.05751	3.56382	18.32388	67.39201
a2	-0.06069	-0.01959	-0.27418	5.83396
a3	0.00067	0.00013	0.00062	-0.92708
a4	-1.4824E-6	1.8476E-7	-1.9939E-6	0.02308
b0	7.75517	7.674	8.23916	7.92459
b1	0.01883	-0.00459	-0.0547	-0.45337

b2	-0.00014	-0.00003	0.00076	0.02339
Chi^2	0.00174	0.0008	0.00081	0.0145
R^2	0.99916	0.99975	0.99975	0.99534

Figure S8. Fitted C_2H_2, C_2H_4, CO_2 and CH_4 isotherms of **1a** measured at 273, 298 and 313 K.

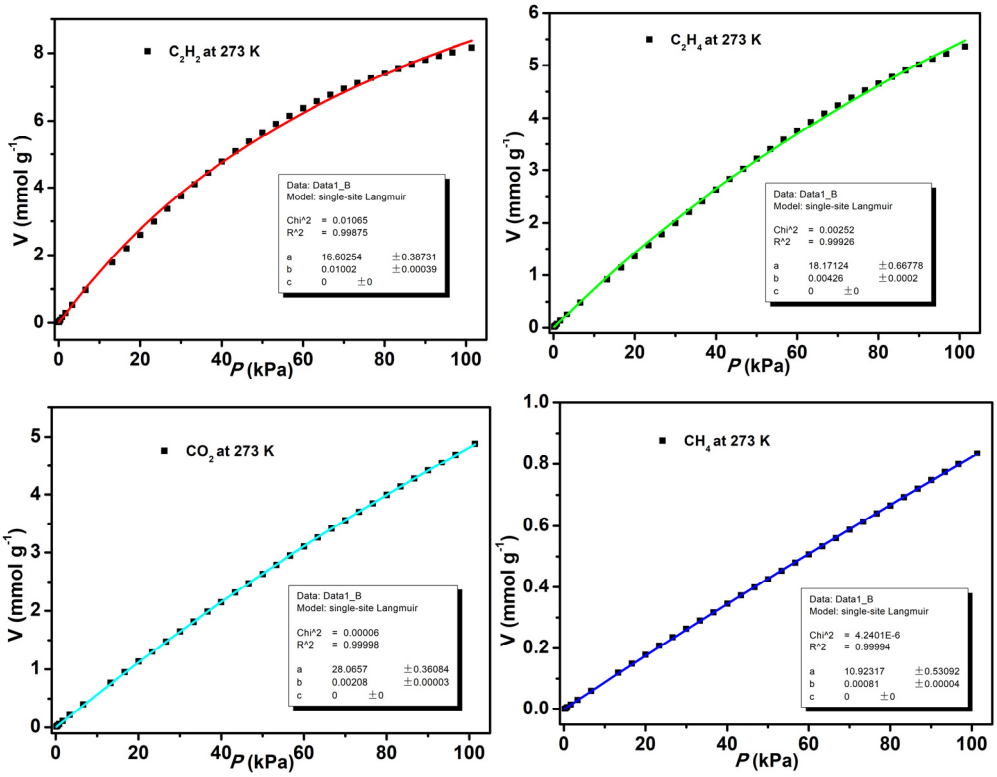

	a	b	Chi^2	R^2
C_2H_2	16.60254	0.01002	0.01065	0.99875
C_2H_4	18.17124	0.00426	0.00252	0.99926
CO_2	28.0657	0.00208	0.00006	0.99998
CH_4	10.92317	0.00081	4.2401E-6	0.99994

Figure S9. C_2H_2, C_2H_4, CO_2, CH_4 adsorption isotherms of **1a** with fitted by single-site Langmuir isotherm model at 273 K.

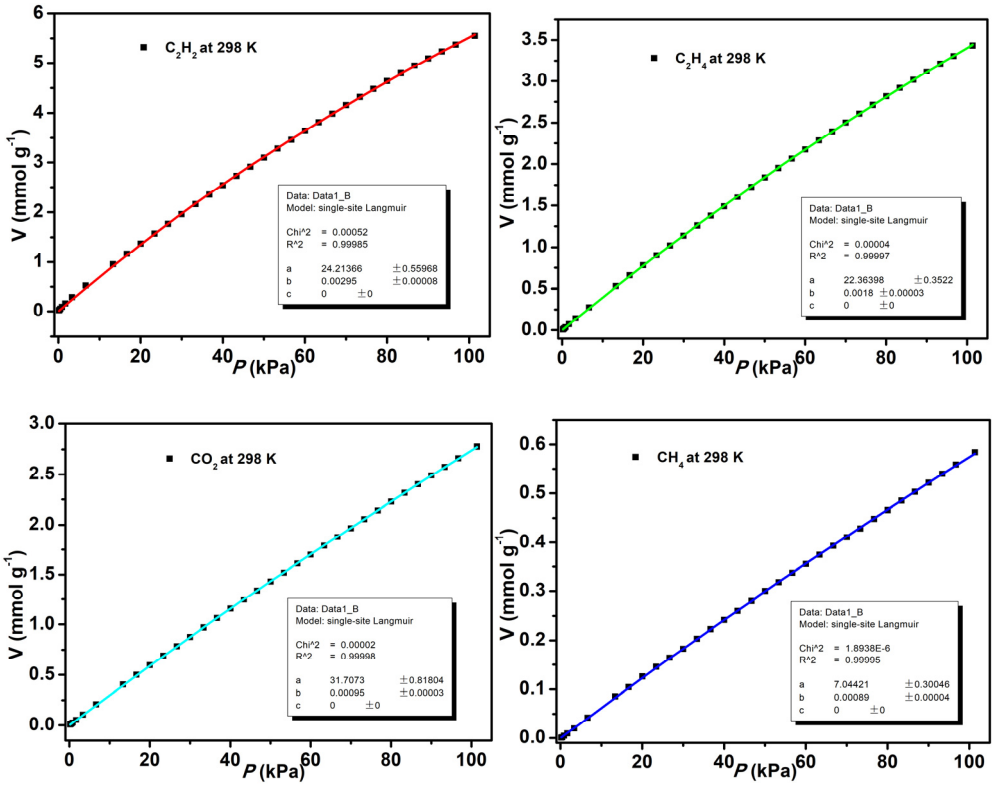

	A1	b1	Chi^2	R^2
C_2H_2	24.21366	0.00295	0.00052	0.99985
C_2H_4	22.36398	0.0018	0.00004	0.99997
CO_2	31.7073	0.00095	0.00002	0.99998
CH_4	7.04421	0.00089	1.8938E-6	0.99995

Figure S10. C_2H_2, C_2H_4, CO_2, CH_4 adsorption isotherms of **1a** with fitted by single-site Langmuir isotherm model at 298 K.

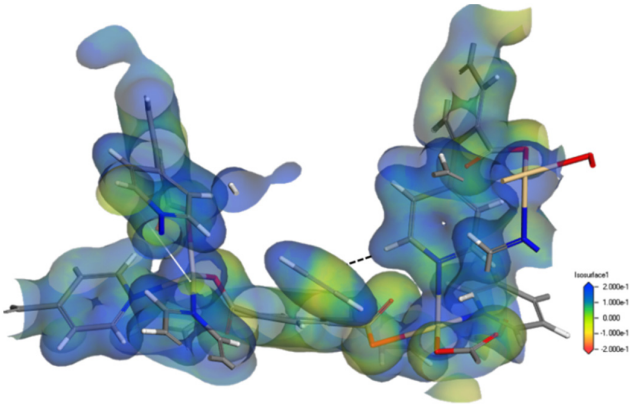

Figure S11. Electrostatic potential of **1a**@C_2H_2 mapped onto the Connolly surface simulated by DMol^3 using GGA (PBE) function.

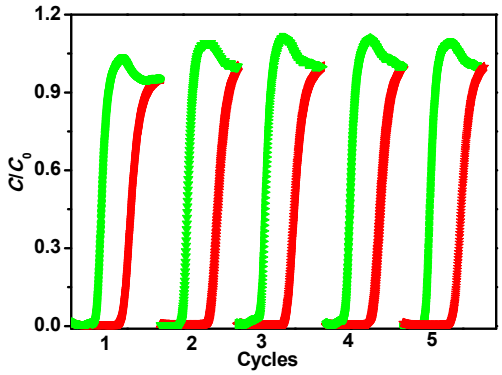

Figure S12. Breakthrough cycling curves for equimolar C_2H_2-CO_2 mixture at room temperature.

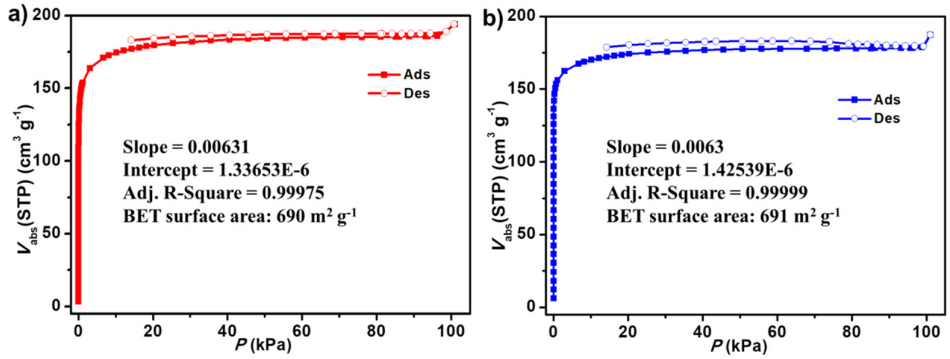

Figure S13. The adsorption isotherm of N_2 at 77K after adsorption experiment (a) and breakthrough experiments (b).

Table S1. Crystal Data and Structure Refinements for **1**.

Chemical formula	$C_{39}H_{29}Cd_2N_5O_{10}$
Formula weight	952.47
T (K)	189(2)
Crystal system, Space group	Monoclinic, *P2(1)/n*
a (Å)	16.9274(13)
b (Å)	22.0209(18)
c (Å)	19.9487(16)
α (°)	90
β (°)	107.005(2)
γ (°)	90
V (Å^3)	7110.9(10)
Z	4

$D_{calcd.}$[g·cm^{-3}]	0.89
μ (mm^{-1})	0.638
Reflns collected/unique/R_{int}	12948/12948/0.0657
Goof	1.031
R_1[a], wR_2[b] [I > 2σ]	R_1 = 0.1076, wR_2 = 0.3034
R_1[a], wR_2[b] (all data)	R_1 = 0.1159, wR_2 = 0.3115

[a]$R_1 = \Sigma(||F_o|-|F_c||)/\Sigma|F_o|$. [b]$R_2 = [\Sigma w(F_o^2 - F_c^2)^2/\Sigma w(F_o^2)^2]^{1/2}$.

Table S2. Selected bond lengths [Å] and angles [°] for **1**.

Cd(1)-N(4)#1	2.283(9)	O(1W)-Cd(1)-O(7)#2	101.9(5)
Cd(1)-O(1)	2.289(8)	N(4)#1-Cd(1)-O(2)	83.1(3)
Cd(1)-O(8)#2	2.301(8)	O(1)-Cd(1)-O(2)	53.2(3)
Cd(1)-N(2)#3	2.325(10)	O(8)#2-Cd(1)-O(2)	136.7(3)
Cd(1)-O(1W)	2.387(11)	N(2)#3-Cd(1)-O(2)	94.2(4)
Cd(1)-O(7)#2	2.485(9)	O(1W)-Cd(1)-O(2)	79.3(4)
Cd(1)-O(2)	2.596(10)	O(7)#2-Cd(1)-O(2)	169.3(3)
Cd(2)-O(5)#4	2.277(7)	O(5)#4-Cd(2)-N(1)	137.6(3)
Cd(2)-N(1)	2.311(8)	O(5)#4-Cd(2)-O(9)	81.7(4)
Cd(2)-O(9)	2.342(10)	N(1)-Cd(2)-O(9)	81.5(4)
Cd(2)-N(3)	2.372(9)	O(5)#4-Cd(2)-N(3)	93.7(3)
Cd(2)-O(3)#3	2.393(11)	N(1)-Cd(2)-N(3)	91.5(3)
Cd(2)-O(4)#3	2.454(11)	O(9)-Cd(2)-N(3)	163.4(4)
Cd(2)-O(6)#4	2.606(7)	O(5)#4-Cd(2)-O(3)#3	87.9(3)
N(4)#1-Cd(1)-O(1)	136.4(3)	N(1)-Cd(2)-O(3)#3	130.3(3)
N(4)#1-Cd(1)-O(8)#2	136.6(3)	O(9)-Cd(2)-O(3)#3	88.9(5)
O(1)-Cd(1)-O(8)#2	85.5(3)	N(3)-Cd(2)-O(3)#3	106.9(4)
N(4)#1-Cd(1)-N(2)#3	94.5(4)	O(5)#4-Cd(2)-O(4)#3	137.1(3)
O(1)-Cd(1)-N(2)#3	88.7(4)	N(1)-Cd(2)-O(4)#3	85.3(3)
O(8)#2-Cd(1)-N(2)#3	97.8(4)	O(9)-Cd(2)-O(4)#3	110.5(5)
N(4)#1-Cd(1)-O(1W)	86.9(4)	N(3)-Cd(2)-O(4)#3	83.7(4)
O(1)-Cd(1)-O(1W)	85.6(4)	O(3)#3-Cd(2)-O(4)#3	52.9(4)
O(8)#2-Cd(1)-O(1W)	85.7(4)	O(5)#4-Cd(2)-O(6)#4	53.7(2)
N(2)#3-Cd(1)-O(1W)	173.2(5)	N(1)-Cd(2)-O(6)#4	85.3(3)
N(4)#1-Cd(1)-O(7)#2	86.3(3)	O(9)-Cd(2)-O(6)#4	80.8(4)
O(1)-Cd(1)-O(7)#2	137.3(3)	N(3)-Cd(2)-O(6)#4	83.6(3)
O(8)#2-Cd(1)-O(7)#2	53.8(3)	O(3)#3-Cd(2)-O(6)#4	141.1(3)
N(2)#3-Cd(1)-O(7)#2	84.9(5)	O(4)#3-Cd(2)-O(6)#4	164.0(3)

Symmetry codes: #1 -x+1, -y+2, -z+1; #2 x-1, y, z; #3 -x+1/2, y-1/2, -z+1/2; #4 -x+1, -y+2, -z; #5-x+1/2, y+1/2, -z+1/2; #6 x+1, y, z

Table S3. Gas adsorption results.

1a	S_{BET} (m^2/g)	Pore sizes	Adsorption uptake ($cm\ g^{-1}$)				Q_{st} ($kJ\ mol^{-1}$)			
			C_2H_2	C_2H_4	CH_4	CO_2	C_2H_2	C_2H_4	CH_4	CO_2
273 K	698	10 Å	182.8	120	18.7	109.4				
298 K			124.4	76.8	13.1	62.2	21.2	18.8	13.8	19.6
313 K			81.5	53.1	9.0	46.6				

Table S4. Comparison of Q_{st} and uptake of C_2H_2 in MOFs at 298 K.

	C_2H_2 Uptake ($mmol\ g^{-1}$)	**C_2H_2 Q_{st} ($kJ\ mol^{-1}$)**	**Ref.**
SNNU-27-Fe_2Co	7.61	20.2	S7
Fe-MOF-74	6.84	47	S8
1a	5.55	20.5	This work
TIFSIX-2-Cu-i	4.1	46.3	S9
FeNi'-MOF	4.29	27	S10
SIFSIX-2-Cu-i	4.02	41.9	S11
PCM-48	3.99	23.6	S12
ZJU-74a	3.84	45	S13
Ni(dpip)	3.73	41.7	S14
Cd(dtztp)	3.58	25	S15
UTSA-100a	3.45	22	S16
UTSA-300a	3.2	57.6	S17
JNU-1	2.89	13	S18
NKMOF-1-Ni	2.72	60.3	S19
ELM-12	2.55	25.4	S20
$[Ni_3(HCOO)_6]$	2.38	40.9	S21
CuI@UiO-66-$(COOH)_2$	2.32	74.5	S22

References

S1 R. Krishna, The Maxwell-Stefan Description of Mixture Diffusion in Nanoporous Crystalline Materials, Microporous Mesoporous Mater. 185 (2014) 30-50.

S2 R. Krishna, Methodologies for Evaluation of Metal-Organic Frameworks in Separation Applications, RSC Adv. 5 (2015) 52269-52295.

S3 R. Krishna, Screening Metal-Organic Frameworks for Mixture Separations in Fixed-Bed Adsorbers using a Combined Selectivity/Capacity Metric, RSC Adv. 7 (2017) 35724-35737.

S4 R. Krishna, Methodologies for Screening and Selection of Crystalline Microporous

Materials in Mixture Separations, Sep. Purif. Technol. 194 (2018) 281-300.

S5 R. Krishna, Metrics for Evaluation and Screening of Metal-Organic Frameworks for Applications in Mixture Separations, ACS Omega 5 (2020) 16987-17004.

S6 L, Wang, W, Sun, Y, Zhang, N, Xu, R, Krishna, J, Hu, Y, Jiang, Y, He, H. Xing, Interpenetration symmetry control within ultramicroporous robust boron cluster hybrid MOFs for benchmark purification of acetylene from carbon dioxide, Angew. Chem. Int. Ed. 60 (2021) 22865-22870.

S7 Y.-Y. Xue, X.-Y. Bai, J. Zhang, Y. Wang, S.-N. Li, Y.-C. Jiang, M.-C. Hu, Q.-G. Zhai, Precise Pore Space Partition Combined with High-Density Hydrogen-Bonding Acceptor within a Metal-Organic Framework for Highly Efficient Acetylene Storage and Separation, Angew. Chem. Int. Ed. 60 (2021) 10122-10128.

S8 E. D. Bloch, W. L. Queen, R. Krishna, J. M. Zadrozny, C. M. Brown, J. R. Long, Hydrocarbon Separations in a Metal-Organic Framework with Open Iron(II) Coordination Sites, Science 335 (2012) 1606-1610.

S9 K.-J. Chen, H. S. Scott, D. G. Madden, T. Pham, A. Kumar, A. Bajpai, M. Lusi, K. A. Forrest, B. Space, J J. Perry IV, M. J. Zaworotko, Benchmark C_2H_2/CO_2 and CO_2/C_2H_2 Separation by Two Closely Related Hybrid Ultramicroporous Materials, Chem 1 (2016) 753-765.

S10 J. Gao, X. Qian, R.-B. Lin, R. Krishna, H. Wu, W. Zhou, B. Chen, Mixed Metal–Organic Framework with Multiple Binding Sites for Efficient C_2H_2/CO_2 Separation, Angew. Chem. Int. Ed. 59 (2020) 4396-4400.

S11 X. Cui, K. Chen, H. Xing, Q. Yang, R. Krishna, Z. Bao, H. Wu, W. Zhou, X. Dong, Y. Han, B. Li, Q. Ren, M. J. Zaworotko, B. Chen, Pore Chemistry and Size Control in Hybrid Porous Materials for Acetylene Capture from Ethylene, Science 353 (2016) 141-144.

S12 J. E. Reynolds III, K. M. Walsh, B. Li, P. Kunal, B. Chen, S. M. Humphrey, Highly selective room temperature acetylene sorption by an unusual triacetylenic phosphine MOF, Chem. Commun. 54 (2018) 9937-9940.

S13 J. Pei, K. Shao, J.-X. Wang, H.-M. Wen, Y. Yang, Y. Cui, R. Krishna, B. Li, G. Qian, A Chemically Stable Hofmann-Type Metal-Organic Framework with Sandwich-Like

Binding Sites for Benchmark Acetylene Capture, Adv. Mater. 32 (2020) 1908275.

S14 Y.-Z. Li, G.-D. Wang, L.-N. Ma, L. Hou, Y.-Y. Wang, Z. Zhu, Multiple Functions of Gas Separation and Vapor Adsorption in a New MOF with Open Tubular Channels, ACS Appl. Mater. Interfaces. 13 (2021) 4102-4109.

S15 G.-D. Wang, Y.-Z. Li, W.-J. Shi, L. Hou, Z. Zhu, Y.-Y. Wang, A new honeycomb metal–carboxylate-tetrazolate framework with multiple functions for CO_2 conversion and selective capture of C_2H_2, CO_2 and benzene, Inorg. Chem. Front. 7 (2020) 1957-1964.

S16 T.-L. Hu, H. Wang, B. Li, R. Krishna, H. Wu, W. Zhou, Y. Zhao, Y. Han, X. Wang, W. Zhu, Z. Yao, S. Xiang, B. Chen, Microporous metal-organic framework with dual functionalities for highly efficient removal of acetylene from ethylene/acetylene mixtures, Nat. Commun. 6 (2015) 7328.

S17 R.-B. Lin, L. Li, H. Wu, H. Arman, B. Li, R.-G. Lin, W. Zhou, B. Chen, Optimized Separation of Acetylene from Carbon Dioxide and MEthylene in a Microporous Material, J. Am. Chem. Soc. 139 (2017) 8022-8028.

S18 H. Zeng, M. Xie,Y.-L. Huang,Y. Zhao, X.-J. Xie, J.-P. Bai, M.-Y. Wan, R. Krishna,W. Lu, D. Li, Induced Fit of C_2H_2 in a Flexible MOF Through Cooperative Action of Open Metal Sites, Angew. Chem., Int. Ed. 58 (2019) 8515-8519.

S19 Y.-L. Peng, T. Pham, P. Li, T. Wang, Y. Chen, K.-J. Chen, K. A. Forrest, B. Space, P. Cheng, M. J. Zaworotko, Z. Zhang, Robust Ultramicroporous Metal-Organic Frameworks with Benchmark Affinity for Acetylene, Angew. Chem. Int. Ed. 57 (2018) 10971-10975.

S20 L. Li, R.-B. Lin, R. Krishna, X. Wang, B. Li, H. Wu, J. Li, W. Zhou B. Chen, Efficient separation of ethylene from acetylene/ethylene mixtures by a flexible-robust metal-organic framework, J. Mater. Chem. A 5 (2017) 18984-18988.

S21 L. Zhang, K. Jiang, J. Zhang, J. Pei, K. Shao, Y. Cui, Y. Yang, B. Li, B. Chen, G. Qian, Low-Cost and High-Performance Microporous Metal-Organic Framework for Separation of Acetylene from Carbon Dioxide, ACS Sustainable Chem. Eng. 7 (2019) 1667-1672.

S22 L. Zhang, K. Jiang, L. Yang, L. Li, E. Hu, L.Yang, K. Shao, H. Xing,Y. Cui,Y. Yang, B. Li, B. Chen, G. Qian, Benchmark C_2H_2/CO_2 Separationinan Ultra-Microporous Metal-Organic Framework via Copper(I)-Alkynyl Chemistry, Angew. Chem. Int. Ed. 60

(2021) 15995-16002.